




Article

ATP13A4 Upregulation Drives the Elevated Polyamine Transport System in the Breast Cancer Cell Line MCF7

Sarah van Veen ^{1,*}, Antria Kourti ¹, Elke Ausloos ¹, Joris Van Asselberghs ², Chris Van den Haute ^{2,3},
Veerle Baekelandt ², Jan Eggermont ¹ and Peter Vangheluwe ^{1,*}

¹ Laboratory of Cellular Transport Systems, Department of Cellular and Molecular Medicine, KU Leuven, 3000 Leuven, Belgium; andria_kourti@hotmail.com (A.K.); elke.ausloos@student.kuleuven.be (E.A.); jan.eggermont@kuleuven.be (J.E.)

² Laboratory for Neurobiology and Gene Therapy, Department of Neurosciences, Leuven Brain Institute, KU Leuven, 3000 Leuven, Belgium; joris.vanasselberghs@kuleuven.be (J.V.A.); chris.vandenhaute@kuleuven.be (C.V.d.H.); veerle.baekelandt@kuleuven.be (V.B.)

³ Leuven Viral Vector Core, KU Leuven, 3000 Leuven, Belgium

* Correspondence: sarah.vanveen@kuleuven.be (S.v.V.); peter.vangheluwe@kuleuven.be (P.V.)

Abstract: Polyamine homeostasis is disturbed in several human diseases, including cancer, which is hallmarked by increased intracellular polyamine levels and an upregulated polyamine transport system (PTS). Thus far, the polyamine transporters contributing to the elevated levels of polyamines in cancer cells have not yet been described, despite the fact that polyamine transport inhibitors are considered for cancer therapy. Here, we tested whether the upregulation of candidate polyamine transporters of the P5B transport ATPase family is responsible for the increased PTS in the well-studied breast cancer cell line MCF7 compared to the non-tumorigenic epithelial breast cell line MCF10A. We found that MCF7 cells presented elevated expression of a previously uncharacterized P5B-ATPase, ATP13A4, which was responsible for the elevated polyamine uptake activity. Furthermore, MCF7 cells were more sensitive to polyamine cytotoxicity, as demonstrated by cell viability, cell death and clonogenic assays. Importantly, the overexpression of ATP13A4 WT in MCF10A cells induced a MCF7 polyamine phenotype, with significantly higher uptake of BODIPY-labeled polyamines and increased sensitivity to polyamine toxicity. In conclusion, we established ATP13A4 as a new polyamine transporter in the human PTS and showed that ATP13A4 may play a major role in the increased polyamine uptake of breast cancer cells. ATP13A4 therefore emerges as a candidate therapeutic target for anticancer drugs that block the PTS.

Keywords: mammalian polyamine transport system; cancer; P5B-type ATPases; ATP13A4



Citation: van Veen, S.; Kourti, A.; Ausloos, E.; Van Asselberghs, J.; Van den Haute, C.; Baekelandt, V.; Eggermont, J.; Vangheluwe, P. ATP13A4 Upregulation Drives the Elevated Polyamine Transport System in the Breast Cancer Cell Line MCF7. *Biomolecules* **2023**, *13*, 918. <https://doi.org/10.3390/biom13060918>

Academic Editors: Manuela Cervelli and Marianna Nicoletta Rossi

Received: 31 March 2023

Revised: 23 May 2023

Accepted: 29 May 2023

Published: 31 May 2023



Copyright: © 2023 by the authors. Licensee MDPI, Basel, Switzerland. This article is an open access article distributed under the terms and conditions of the Creative Commons Attribution (CC BY) license (<https://creativecommons.org/licenses/by/4.0/>).

1. Introduction

Polyamines, such as spermidine and spermine, are ubiquitous organic polycations that are involved in a broad range of critical cellular functions, including gene expression, cell proliferation and differentiation. Intracellular polyamine levels are tightly regulated by the concerted action of biosynthesis, catabolism and polyamine transport. Whereas polyamine metabolism has been well characterized, the molecular players of the mammalian polyamine transport system (PTS) are only now emerging. Our group recently characterized ATP13A2 and ATP13A3, two isoforms of the P5B-type transport ATPases (ATP13A2-5), as members of the PTS [1]. ATP13A2 works as a lysosomal polyamine exporter of endocytosed polyamines that contributes to cellular polyamine uptake and is implicated in neurodegenerative disorders [2]. ATP13A3 has been genetically linked with pulmonary arterial hypertension and is a major component of the mammalian PTS that is mutated and defective in the commonly used CHO-MG cell model, which is marked by a deficient PTS [3]. P5B ATPases share high sequence similarity in the substrate

binding site, suggesting that also the ATP13A4 and ATP13A5 isoforms may function as polyamine transporters.

Polyamine homeostasis is disturbed in several human diseases, including neurodegeneration [2] and cancer [4]. Various cancers, including breast cancer, are hallmarked by increased intracellular polyamine levels as a consequence of upregulated polyamine biosynthesis and PTS activity [5–8]. Elevated polyamine content correlates with cancer aggressiveness and is linked to a poor prognosis for breast cancer patients [5]. This is also the case for high expression of ornithine decarboxylase (ODC, the key rate-limiting enzyme in polyamine synthesis) [6]. High levels of polyamines are associated with hyperproliferation and tumorigenesis through effects on various signaling cascades, such as the mitogen-activated protein kinase (MAPK) [4,9,10] and PI3K/AKT/mTOR pathways [11]. Estrogens, known to play a major role in breast cancer development and progression, stimulate ODC expression and activity [12]. In addition, the breast cancer oncogenes MYC [13] and PI3KCA [14] increase the polyamine load by stimulating ODC-mediated polyamine synthesis and the PTS. Thus far, the contributing polyamine transporters remain unidentified, despite the fact that the PTS has become a promising target for cancer therapy. Polyamine transport inhibitors, such as AMXT-1501, that block cellular polyamine uptake [15] are currently being tested in clinical trials in the context of breast cancer (clinicaltrials.gov, NCT05500508). In addition, polyamine analogs that utilize the PTS and disrupt polyamine metabolism are considered a novel therapeutic strategy for breast cancer [12].

In the present study, we investigated the putative role of P5B ATPases in polyamine homeostasis in the human cell lines MCF7 and MCF10A, which are commonly used *in vitro* models in breast cancer research. MCF10A is a spontaneously immortalized, normal-like breast epithelial cell line derived from fibrocystic mammary tissue [16], whereas MCF7 is the most studied breast cancer cell line worldwide and was generated from pleural effusions from a patient with metastatic breast cancer [17]. MCF7 is estrogen-receptor-positive and belongs to the luminal A breast cancer subtype [18]. Interestingly, we found higher expression of ATP13A4 in the MCF7 cells as compared to the MCF10A cells, which contributed to increased polyamine uptake and cytotoxicity, as well as the activation of MAPK signaling. Our study is the first to characterize ATP13A4 as a polyamine transporter that plays a role in the PTS of MCF7 breast cancer cells. Our work provides a stepping stone to further establish the potential of ATP13A4 as a therapeutic candidate in cancer.

2. Materials and Methods

2.1. Materials

The following reagents were purchased from Merck: dimethyl sulfoxide (DMSO; 276855), difluoromethylornithine (DFMO; D193), 4-methylumbelliferyl heptanoate (MUH; M2514), crystal violet (V5265), berenil (D7770), SigmaFast™ protease inhibitor (S8820), benzyl viologen dichloride (271845), putrescine dihydrochloride (P7505), spermine (S3256) and spermidine (S2626). Bovine serum albumin (BSA; 3854.3) was ordered from Carl Roth. N-(3-aminopropyl)cyclohexylamine (APCHA; sc-202715) and trans-4-methylcyclohexylamine (4MCHA; sc-272662) were obtained from Santa Cruz Biotechnology. TrypLE™ (12604021) and paraformaldehyde (J61899.AP) were ordered from ThermoFisher Scientific. The following antibodies were purchased from Cell Signaling Technology: phospho-JNK antibody (9251), phospho-AKT antibody (4058), phospho-ERK1/2 antibody (9101), HRP-linked anti-mouse IgG antibody (7076) and HRP-linked anti-rabbit IgG antibody (7074). Anti-GAPDH antibody (G8795) was purchased from Merck. Methylglyoxal bisguanylhydrazine (MGBG) and boron dipyrromethene (BODIPY)-conjugated polyamines [19] were supplied by Dr. P. van Veldhoven and Dr. S. Verhelst, respectively.

2.2. Preparation of Polyamines and Inhibitors

Polyamines were dissolved in 0.1 M MOPS (pH 7.0, KOH) to a final stock concentration of 500 mM (putrescine, spermidine) or 200 mM (spermine). The polyamine synthesis inhibitors 4MCHA and APCHA were diluted in DMSO to a final stock concentration

of 500 mM. DFMO (500 mM), berenil (200 mM), benzyl viologen (200 mM) and MGBG (100 mM) were prepared in milliQ water to a final stock concentration as indicated between brackets. BODIPY-labeled polyamines were dissolved in 0.1 M MOPS-KOH (pH 7.0) to a final stock concentration of 5 mM.

2.3. Cell Culture and Lentiviral Transduction

The cell lines MCF10A (CRL-10317) and MCF7 (HTB-22) were purchased from ATCC. MCF7 cells were cultured in Dulbecco's Modified Eagle Medium (DMEM; Gibco) supplemented with 10 % heat-inactivated fetal bovine serum (FBS; PAN BioTech), 1% penicillin/streptomycin (Merck, Rahway, NJ, USA), 1% non-essential amino acids (Merck) and GlutaMAX™ (Thermo Fisher Scientific, Waltham, MA, USA). MCF10A cells were cultured in DMEM/F-12 medium (Thermo Fisher Scientific) supplemented with 5 % heat-inactivated horse serum (Merck), EGF (20 ng mL⁻¹; PeproTech EC Limited, London, UK), hydrocortisone (0.5 µg mL⁻¹; TCI Europe, Zwijndrecht, Belgium), cholera toxin (100 ng mL⁻¹; Merck), insulin (10 µg mL⁻¹; Merck), 1% penicillin/streptomycin (Merck), 1% non-essential amino acids (Merck) and GlutaMAX™ (Thermo Fisher Scientific). Note that we used heat-inactivated FBS or horse serum to deplete the polyamine oxidase activity, which may otherwise affect the supplemented fluorescent polyamine probes or polyamines. To prevent serum polyamine oxidase activity, heat inactivation is preferred over aminoguanidine treatment to avoid the aminoguanidine-dependent inhibition of NO synthase [20], which plays a key role in endosomal polyamine uptake [21,22]. MCF7 and MCF10A cells were cultured at 37 °C with 5% CO₂. All cell lines were routinely tested for mycoplasma infection and found to be negative.

MCF10A cells with stable overexpression of human ATP13A4 WT or the catalytically dead mutant D486N were produced via lentiviral vector transduction. After lentiviral transduction, cells were selected with 1 µg mL⁻¹ puromycin.

2.4. RT-qPCR

The mRNA expression levels of ATP13A2-4 were quantified by RT-qPCR analysis. Therefore, we extracted RNA from 1.0 × 10⁶ cells using the NucleoSpin RNA Plus Kit (740984, Macherey-Nagel, Düren, Germany) according to the manufacturer's instructions. The concentration and purity of the RNA samples were measured using a Nanodrop spectrophotometer (Thermo Fisher), followed by the conversion of RNA into cDNA using the RevertAid H Minus First Strand cDNA Synthesis Kit (K1631, Thermo Fisher). The cDNA was then subjected to SYBR Green-based qPCR with gene-specific primer pairs (Table 1). β-actin was used as a reference gene. The analysis was performed using a Light Cycler machine (Roche) and the cycling conditions were as follows: 10 min at 95 °C, 50 cycles: 10 s at 95 °C, 30 s at 55 °C, 1 min at 95 °C and 1 min at 55 °C. Melting curves were analyzed from 55 to 95 °C. Finally, the mean Cq values were determined.

Table 1. Gene accession numbers and primer sequences.

Gene	NCBI Accession Number	Primer Sequences
γ-actin	NM_001199954.3	F: CACTGAGCGAGGCTACAGCTT R: TTGATGTTCGCGCACGATTT
ATP13A2	XM_005245810	F: CATGGCTCTGTACAGCCTGA R: CTCATGAGCACTGCCACTGT
ATP13A3	XM_047448904	F: TACTGTGGAGCACTGATG R: GAGTTGCCACCATGTCATGC
ATP13A4	XM_047449063	F: CCAGCACGCTCTGCTCAATG R: GAAGATGGATCCGGCAAGGC

2.5. BODIPY-Polyamine Uptake

For the flow-cytometry-based measurement of BODIPY-polyamine uptake, cells were seeded in 12-well plates at a density of 1.0×10^5 cells per well. The next day, cells were incubated for 2 h with 1 μ M BODIPY-conjugated polyamines, i.e., putrescine, spermidine and spermine. To evaluate the effect of inhibitors of polyamine uptake or synthesis, the cells were pre-treated with 1 mM benzyl viologen (90 min) or 10 μ M MGBG (30 min), respectively. Afterwards, cells were washed and resuspended in PBS supplemented with 1% BSA. Uptake was measured by recording the mean fluorescence intensities (MFI) of 10,000 events using a flow cytometer (ID7000 spectral cell analyzer, Sony).

For the confocal-microscopy-based analysis of BODIPY-polyamine uptake, cells were seeded on cover slips in 12-well plates at a density of 5.0×10^4 cells per well. The next day, cells were incubated for 2 h with 1 μ M BODIPY-conjugated polyamines, washed in PBS and fixed in 4% paraformaldehyde for 30 min at 37 °C. Thereafter, cells were washed in PBS and stored at 4 °C. The next day, cells were stained with DAPI to visualize the nuclei. Cover slips were mounted on slides and images were acquired using an LSM880 confocal microscope (Zeiss, Jena, Germany) with a 63 \times objective.

2.6. Measurement of Cell Viability and Cell Death

Cells were seeded in 96-well plates (1.0×10^4 cells per well) and, the following day, cells were treated with increasing concentrations of the different polyamines and inhibitors for 24 h to 1 week, as indicated. For the 1-week treatments, we plated 5.0×10^3 cells per well, and, every 48 h, we replaced the medium containing the respective inhibitor. Following the incubation period, we assessed cell death (ToxiLight assay, Lonza, LT07-117) and cell viability (MUH cell viability assay [2]).

2.7. Colony Formation Assay

Cells were seeded in a 12-well plate (MCF7: 5.0×10^3 cells per well, MCF10A: 1.0×10^3 cells per well) and were treated the next day with indicated concentrations of spermidine or spermine. Every 5 days, the medium was discarded and new medium containing the treatment of interest was added. After 14 days, the medium was removed and cells were washed with PBS. The cells were fixed with methanol for 15 min and then stained with 0.01% (*w/v*) crystal violet solution in milliQ water for 1 h. Afterwards, the plates were carefully rinsed with distilled water and left to dry at room temperature. An ordinary scanner was used to capture images of the 12-well plates. To quantify the staining (relative to the untreated control condition), crystal violet was solubilized from the stained colonies using 10% acetic acid (1 h incubation with gentle rocking, room temperature) and absorbance was read at 590 nm, as described in [23].

2.8. Western Blotting

Cells were seeded in 10 cm plates (1.0×10^6 cells per plate) and, the following day, cells were treated with spermidine (100 μ M) or spermine (100 μ M) for indicated times. Thereafter, cells were dissociated from the plates using TrypLE™ and lysed in RIPA buffer supplemented with protease and phosphatase inhibitors (A32957, Thermo Fisher Scientific). Proteins in cell lysates (20–40 μ g) were separated on precast NuPAGE™ 4–12% Bis-Tris gels (Invitrogen, Waltham, MA, USA) using MES (Figure 4 and Figure S5) or MOPS (Figure 3A) running buffer (Life Sciences), followed by transfer onto polyvinylidene fluoride (PVDF) membranes (Thermo Fisher Scientific) according to the manufacturer's instructions. After blocking in TBS-T (50 mM Tris-HCl, 150 mM NaCl, pH 7.5, 0.1% Tween-20 (Sigma, St. Louis, MO, USA)) supplemented with 5% non-fat dry milk, blots were incubated with primary antibodies (1/1000 dilution in TBS-T with 1% BSA) and horseradish peroxidase (HRP)-conjugated anti-rabbit secondary antibodies (1–2 h; 1/1000 dilution in TBS-T with 1% BSA). We used primary antibodies directed against phospho-JNK, phospho-ERK1/2, phospho-AKT, ATP13A4 and GAPDH. The rabbit polyclonal anti-ATP13A4 antibody was home-made and raised against the epitope ¹¹⁸²VSYSNP VFESNEEQL. Blots were incubated

with phospho-specific antibodies overnight at 4 °C, whereas the incubation time for anti-ATP13A4 and anti-GAPDH antibodies was 1 h at room temperature. Protein expression was detected using an enhanced chemiluminescence (ECL) substrate (Thermo Fisher Scientific) and the Bio-Rad ChemiDoc MP imaging system. Quantification was performed with the ImageJ software (<https://imagej.net/ij/index.html> (accessed on 30 May 2023)).

2.9. Statistical Analysis

Data analysis was performed using GraphPad Prism 9 (La Jolla, CA, USA). Figure legends cover the type of statistical test used. Data are presented as the mean \pm s.e.m., and, in the bar graphs, individual points are also shown. Each experiment was repeated at least three times, except for that presented in Figure S4 (N = 2).

3. Results

The tumorigenic human breast cancer cell line MCF7 presents upregulated PTS activity compared to the non-tumorigenic epithelial breast cell line MCF10A [24], but the molecular players responsible for this phenotype remain unknown. Here, we hypothesize that isoforms of the P5B transport ATPases may be implicated.

3.1. MCF7 Cells Show Enhanced PTS Activity Compared to MCF10A Cells

First, we confirmed, via cellular uptake experiments with the fluorescent BODIPY-labeled putrescine, spermidine and spermine, that MCF7 cells present an elevated PTS compared to MCF10A cells (Figure 1).

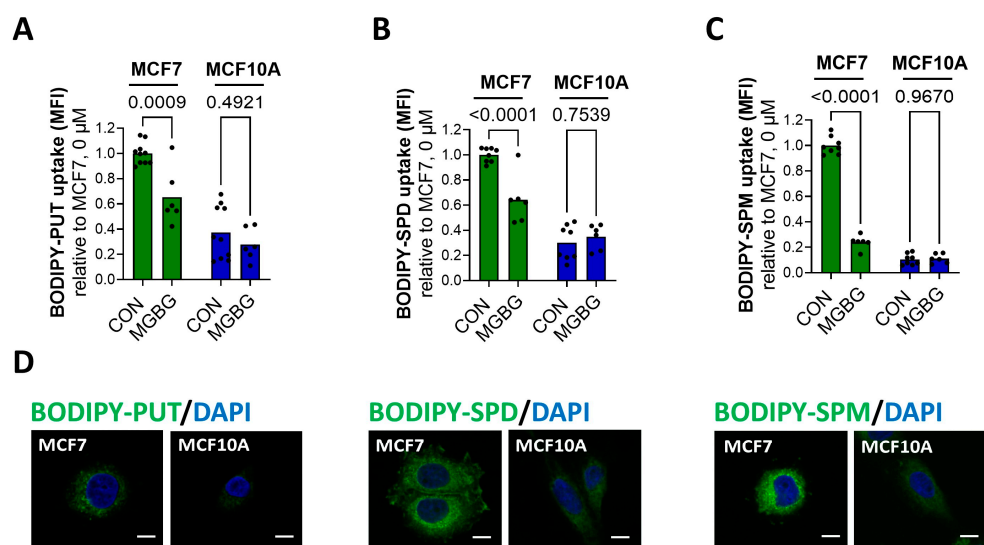


Figure 1. MCF7 cells exhibit an upregulated PTS and higher expression of ATP13A4 compared to MCF10A cells. Cellular uptake of BODIPY-labeled putrescine (BODIPY-PUT) (A,D), spermidine (BODIPY-SPD) (B,D) and spermine (BODIPY-SPM) (C,D) (1 μM, 2 h) in MCF7 versus MCF10A cells was assessed via flow cytometry (A–C) or confocal microscopy (D). Representative confocal microscopy images are shown of three independent experiments. Scale bar, 10 μm. MFI, mean fluorescence intensity. Data in the bar graphs are presented as the mean of minimal three independent experiments, with individual data points shown. Statistical significance was determined by one-way ANOVA with Šidák’s multiple comparisons test (A–C). *p* values are depicted in the graphs.

Flow-cytometry-based uptake experiments revealed the over three-fold higher uptake of BODIPY-labeled putrescine (Figure 1A) and spermidine (Figure 1B) in MCF7 cells compared to MCF10A cells, whereas the uptake of BODIPY-spermine was over ten-fold higher (Figure 1C). These findings were confirmed by confocal fluorescent microscopy (Figure 1D). Whereas we observed strong fluorescence in the MCF7 cells incubated with BODIPY-polyamines, only weak fluorescent intensity was detected in the MCF10A cells. The difference between the cell lines was highest for BODIPY-labeled spermine (Figure 1D, bottom panels). Furthermore, to prove that the fluorescent probes entered the cell via the PTS, we investigated the impact of methylglyoxal bis-(guanylhydrazone) (MGBG), a spermidine analog that is taken up via the PTS, competing with the cellular uptake of polyamines, and benzyl viologen (BV), a commonly used PTS inhibitor [3,24,25]. Both MGBG (10 μ M, 30 min pre-treatment) and BV (1 mM, 90 min pre-treatment) significantly reduced the uptake of BODIPY-labeled putrescine (Figure 1A and Figure S1A), spermidine (Figures 1B and S1B) and spermine (Figure 1C and Figure S1C) in the MCF7 cells, but not in MCF10A cells. These findings suggest that, in sharp contrast to the MCF7 cells, MCF10A cells only have minimal PTS activity.

To further assess the importance of the PTS, we compared the sensitivity of the MCF7 and MCF10A cell lines to BV by measuring cell viability using the MUH assay. Interestingly, the MCF7 cells demonstrated increased cytotoxicity following 48 h treatment with BV, compared to MCF10A cells (Figure S1D), indicating that the MCF7 cells rely more on a functional PTS to maintain their overall health.

Altogether, our data show that the PTS is upregulated in MCF7 cells versus MCF10A cells.

3.2. The P5B ATPase ATP13A4 Is Upregulated in MCF7 versus MCF10A Cells

To test whether specific P5B ATPase isoforms play a role in MCF7 cells, we evaluated the relative expression of ATP13A2-5 between the cell lines by mining the ARCHS4 web resource of RNA-seq data [26] as a starting point (Figure 2A,B). All P5B ATPases are expressed in MCF7 and MCF10A cells (Figure 2B), with ATP13A2 and ATP13A3 presenting similarly high expression levels in both cell lines, whereas ATP13A4 and ATP13A5 are expressed to a lesser extent, but with higher expression in MCF7 versus MCF10A cells. Of note, MCF7 appears amongst the highest ATP13A4-expressing cell lines (Figure 2A).

To corroborate this finding, we performed qPCR to assess the mRNA levels of the P5B ATPases ATP13A2-5 in MCF7 and MCF10A cells (Figure 2C–E) and confirmed that MCF7 cells presented significantly higher ATP13A4 mRNA levels than MCF10A cells, with an almost tenfold difference in expression (Figure 2E). Surprisingly, the expression of ATP13A2 and ATP13A3 was significantly lower in MCF7 than in MCF10A cells (Figure 2C,D), whereas we were unable to detect ATP13A5 mRNA in both cell lines. Furthermore, we investigated the expression of ATP13A2-4 at the protein level by performing a Western blot analysis. Unfortunately, the commercially available antibodies against ATP13A2-4 were not able to detect endogenous protein levels in MCF10A and MCF7 cells.

Based on this comparison, ATP13A4 emerges as a candidate polyamine transporter that may be responsible for the increased PTS in MCF7 cells.

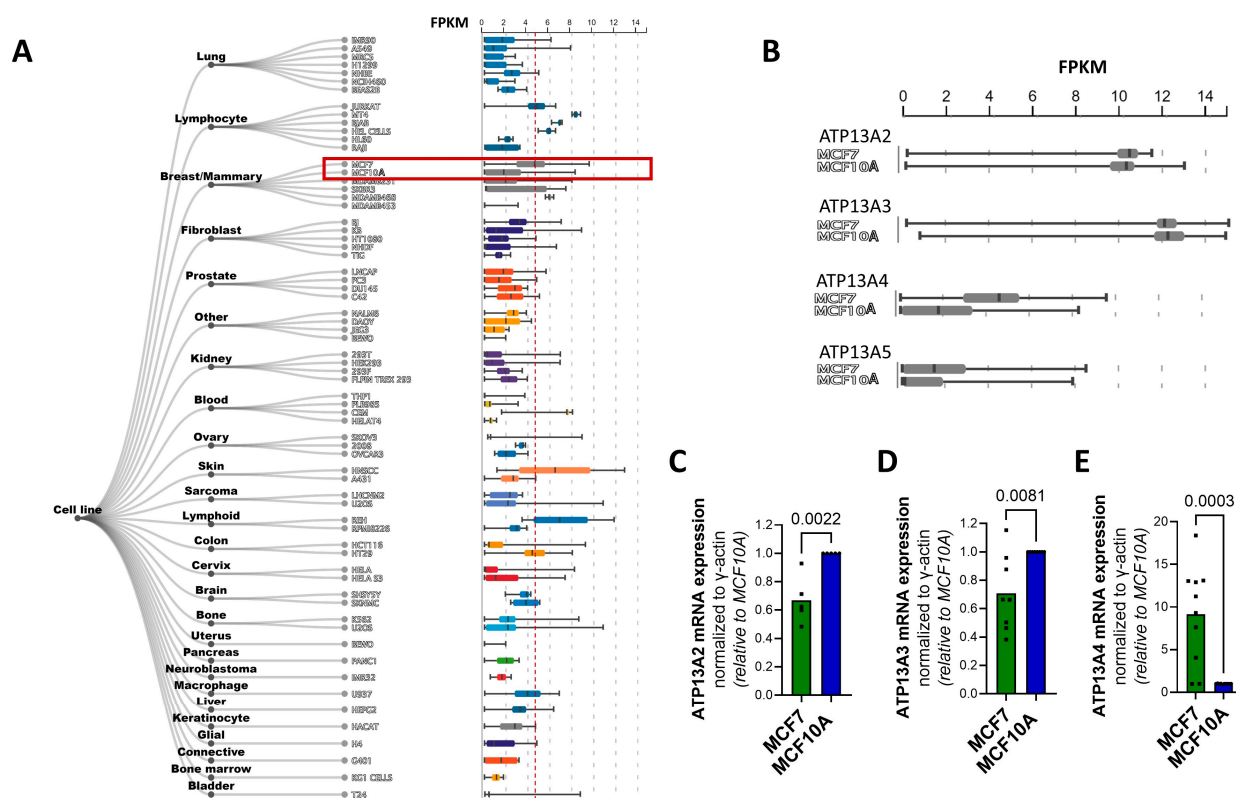


Figure 2. mRNA levels of P5B ATPase isoforms in MCF7 and MCF10A cell lines. Boxplots obtained from ARCHS4 [26], a web resource of processed RNA-seq data, showing mRNA expression levels of (A) ATP13A4 in different cell lines and (B) of P5B ATPases ATP13A2-5 in MCF7 versus MCF10A cells. Expression of ATP13A2 (C), ATP13A3 (D) and ATP13A4 (E) was evaluated at the mRNA level via qPCR. mRNA expression was normalized to β -actin. Data in the bar graphs are presented as the mean of minimal three independent experiments, with individual data points shown. Statistical significance was determined by unpaired two-tailed *t*-test (C–E). *p* values are depicted in the graphs.

3.3. MCF7 Cells Are More Sensitive to Polyamine Cytotoxicity

At high concentrations, polyamines become toxic, and, here, we investigated the relative cytotoxicity of exogenous polyamines in the MCF7 and MCF10A cell lines as a complementary readout of the PTS activity (Figure 3).

First, we treated MCF10A and MCF7 cells for 24 h with increasing concentrations of putrescine, spermidine and spermine to assess their impacts on cell viability. As shown in Figure 3A–C, MCF10A cells were insensitive to the tested polyamines, in line with low PTS activity. In contrast, MCF7 cells showed lower viability following treatment with spermine (Figure 3C) and, to a lesser extent, spermidine (Figure 3B), but not putrescine (Figure 3A). In addition, we assessed cell death following exposure to spermine with the ToxiLight cytotoxicity assay, which measures adenylate kinase, an enzyme that is released by dying cells. High levels of spermine led to increased cell death in MCF7 cells, whereas no cell death was observed in MCF10A cells (Figure 3D). These data are in line with the cell viability results (Figure 3C), implying that the reduced cell viability in MCF7 cells following spermine treatment is due to increased cell death.

Furthermore, we cross-validated the polyamine cytotoxicity data via colony formation assays (Figure 3E–J), evaluating the impact of each polyamine on the ability of a single cell to proliferate and grow into a colony. The polyamines spermidine (Figure 3G,H) and especially spermine (Figure 3I–J) inhibited colony formation more severely in MCF7 cells than in MCF10A cells, which appeared more resistant. Putrescine did not differentially impact clonogenic ability (Figure 3E,F).

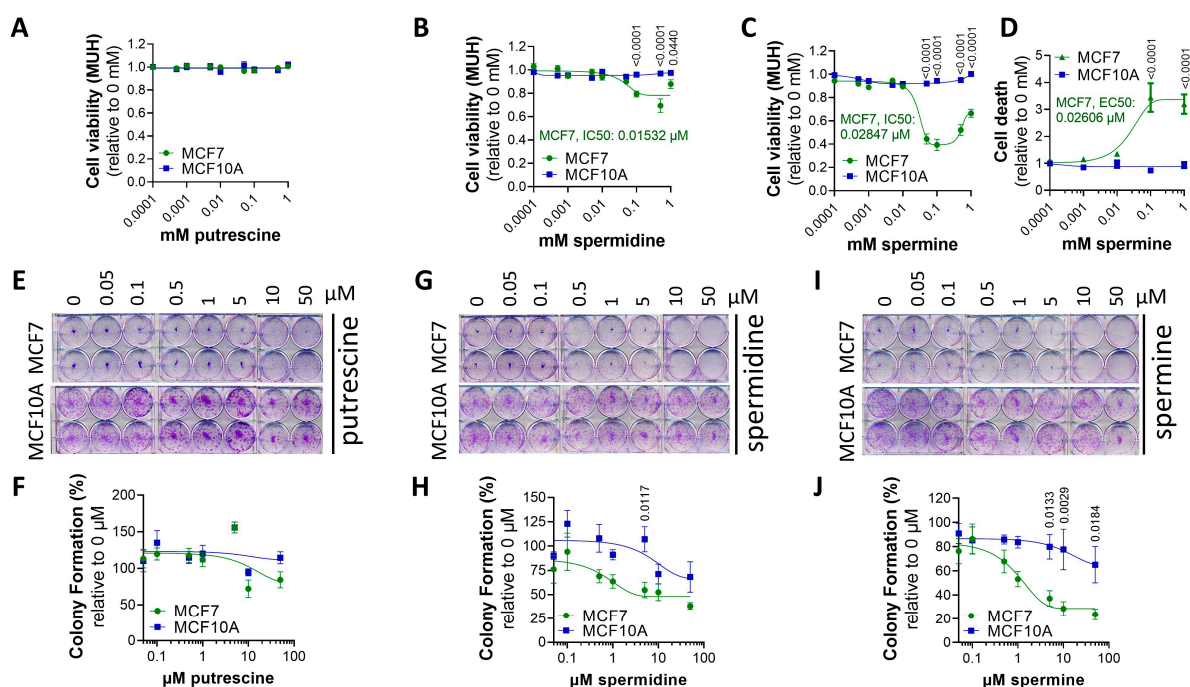


Figure 3. MCF7 cells are more sensitive to polyamine cytotoxicity than MCF10A cells. MCF7 and MCF10A cells were treated for 24 h (A–D) or 2 weeks (E–J) with indicated concentrations of putrescine (PUT) (A), spermidine (SPD) (B) and spermine (SPM) (C,D). Cell viability and cell death were assessed via MUH assay (A–C) and Toxilight (D) assay, respectively. Colony formation ability was evaluated via clonogenic assays (E,G,I) and quantified based on crystal violet absorbance (590 nm) (F,H,J). (E,G,I) depict representative pictures of at least three independent experiments. Data were normalized to untreated controls for each cell line and are presented as the mean \pm s.e.m. of at least three independent experiments. Statistical significance was determined by two-way ANOVA with Šídák’s multiple comparisons test. *p* values are depicted in the graphs; non-significant values are not indicated.

To examine the role of polyamine metabolism, we compared the effects of pharmacological inhibitors of the polyamine metabolic pathway (Figure S2A) on the cell viability of MCF7 and MCF10A cells, which have previously been considered for cancer therapy. MCF7 cells appeared more sensitive to the inhibition of the polyamine synthesis pathway after treating the cells for one week with DFMO (ornithine decarboxylase inhibitor), 4MCHA (spermidine synthase inhibitor) or APCA (spermine synthase inhibitor), and less sensitive to MGBG (*S*-adenosyl-*L*-methionine-decarboxylase inhibitor), although the differences were mild (Figure S2B–E). In addition, after one week of incubation, MCF7 cells were also slightly more sensitive to berenil, which inhibits SAT1, a key enzyme in polyamine catabolism (Figure S2F). The overall comparable sensitivity to polyamine metabolism inhibitors indicates that polyamine metabolism may not be notably different between the two cell lines.

All in all, our findings demonstrate that MCF7 cells are more sensitive to polyamine cytotoxicity, particularly spermine, than MCF10A cells, whereas polyamine metabolism blockers do not have a strong differential impact.

3.4. Overexpression of ATP13A4 in MCF10A Cells Induces an MCF7 Polyamine Phenotype

To investigate the causal role of ATP13A4 in the differential polyamine phenotypes of MCF7 and MCF10A cells, we overexpressed ATP13A4 in MCF10A to recapitulate the polyamine phenotype of MCF7 cells. Therefore, we generated stable MCF10A cells with the overexpression of ATP13A4 via lentiviral transduction (WT or a transport dead mutant D486N that was mutated in the catalytic site for autophosphorylation) (Figure 4A).

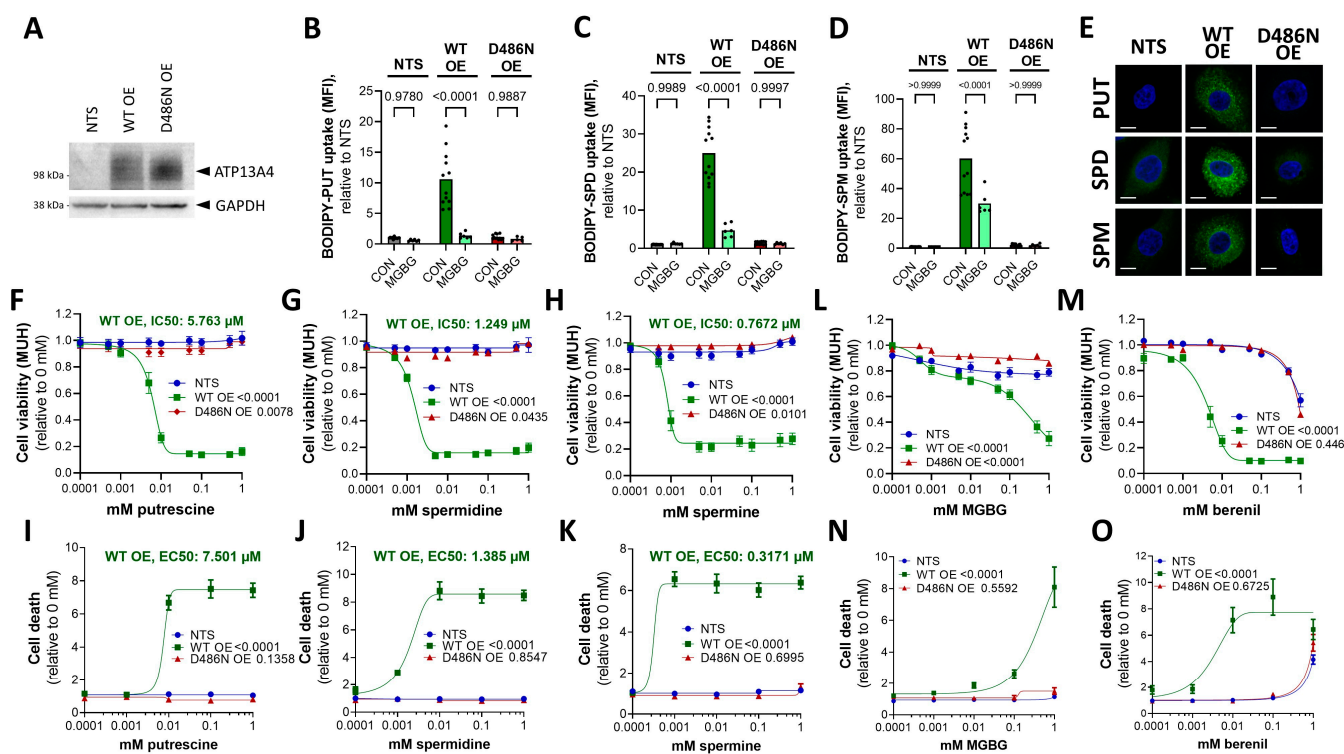


Figure 4. Overexpression of ATP13A4 WT in MCF10A cells induces an MCF7 polyamine phenotype. (A) Immunoblot depicting ATP13A4 overexpression levels in MCF10A cells (non-transduced, NTS; ATP13A4 WT overexpression, WT OE; ATP13A4 D486N mutant overexpression, D486N OE). Cellular uptake of BODIPY-labeled putrescine (BODIPY-PUT) (B,E), spermidine (BODIPY-SPD) (C,E) and spermine (BODIPY-SPM) (D,E) (1 μ M, 2 h) was assessed via flow cytometry (B–D) or confocal microscopy (E). Representative confocal microscopy images are shown of three independent experiments. Scale bar, 10 μ m. MFI, mean fluorescence intensity. Cells were treated for 24 h with indicated concentrations of putrescine (F,I), spermidine (G,J), spermine (H,K), MGBG (L,N) or berenil (M,O) prior to cell viability (MUH; (F–H,L,M)) or cell death (Toxilight; (I–K,N,O)) assays. Data were normalized to untreated controls for each cell line and are presented as the mean of at least three independent experiments, with individual data points shown (B–D), or \pm s.e.m. (F–O). Statistical significance was determined by one-way ANOVA with Šídák’s multiple comparisons test (B–D) or by two-way ANOVA with Dunnett’s multiple comparisons test ((F–O), compared to NTS). *p* values are depicted in the graphs.

Interestingly, the uptake of all BODIPY-labeled polyamines was significantly increased in MCF10A cells as a consequence of the ATP13A4 WT overexpression, with the largest uptake effect on BODIPY-spermine (60-fold) over BODIPY-spermidine (25-fold) and BODIPY-putrescine (10-fold), as compared to non-transduced MCF10A cells (Figure 4A–D). In addition, the higher cellular uptake of BODIPY-polyamines was not observed with the D486N mutant, demonstrating that the catalytic transport activity of ATP13A4 is required (Figure 4B–D). The higher uptake of BODIPY-labeled polyamines in MCF10A cells that overexpressed ATP13A4 WT was confirmed by confocal microscopy (Figure 4E). Furthermore, MGBG significantly reduced the uptake of BODIPY-labeled putrescine (Figure 4B), spermidine (Figure 4C) and spermine (Figure 4D) in MCF10A cells with the overexpression of ATP13A4 WT, but not in non-transduced or D486N-expressing MCF10A cells. Altogether, we present here the first evidence that ATP13A4 functions as a polyamine transporter within the mammalian PTS that may present broad polyamine specificity.

To complement our findings of polyamine uptake in the MCF10A cell lines, we examined polyamine cytotoxicity, which, in MCF7 cells, is correlated with the elevated PTS (Figure 3). ATP13A4 WT overexpression strongly sensitized MCF10A cells to putrescine

(Figure 4F,I), spermidine (Figure 4G,J) and spermine (Figure 4H,K), as evidenced by the reduced cell viability and increased cell death. Of note, spermine exhibited the lowest IC50 (0.7672 μ M) and EC50 (0.371 μ M) values, followed by spermidine (IC50: 1.249 μ M, EC50: 1.385 μ M) and putrescine (IC50: 5.763 μ M, EC50: 7.501 μ M). These phenotypes are not observed in non-transduced MCF10A cells or cells overexpressing the catalytically inactive D486N mutant (Figure 4F–K), which confirms that the polyamine transport activity plays a role. Note that MCF10A cells were cultured with 5% heat-inactivated horse serum, which contains extremely low levels of polyamine oxidase [27,28] that is also inactivated by heat inactivation. Since the polyamine toxicity in MCF10A was only observed upon ATP13A4 WT overexpression, we can safely attribute the observed polyamine toxicity phenotypes to ATP13A4-dependent polyamine uptake and not to polyamine oxidases in the serum. In addition, the overexpression of ATP13A4 WT, but not the D486N mutant, sensitized MCF10A cells to MGBG toxicity, in line with the increased PTS activity (Figure 4L,N). Remarkably, these cells also become highly sensitive to SAT1 inhibition via berenil, pointing to a protective role of SAT1-mediated polyamine degradation in these cells (Figure 4M,O). Of note, the cytotoxicity phenotypes are much more pronounced in the MCF10A cells than in the MCF7 cells, most likely as a consequence of the high ATP13A4 overexpression levels. This may also explain the observed putrescine toxicity, which was not observed in the MCF7 cells. Lastly, we did not observe a reducing effect of BV on BODIPY-polyamine uptake in ATP13A4-overexpressing MCF10A cells or an impact on viability, indicating that BV may not be a direct inhibitor of ATP13A4 (Figure S3).

Together, our findings with polyamine uptake and cytotoxicity assays indicate that overexpressing ATP13A4 WT in MCF10A cells confers a polyamine uptake phenotype resembling MCF7 cells with high endogenous ATP13A4 expression, indicating that ATP13A4 is the driver of the increased PTS in MCF7 breast cancer cells.

3.5. ATP13A4 Overexpression Triggers Activation of the JNK Signaling Pathway in MCF10A Cells

One of the most commonly altered pathways driving breast cancer cell progression is the PI3K/AKT/mTOR signaling cascade [29], whereas also the N-terminal c-Jun kinase (JNK) [29] and extracellular-signal-regulated kinase (ERK) [29] in the MAPK pathway have been implicated [10]. Moreover, the interplay between these signaling pathways and polyamines has been described before [4,14,30]. Therefore, we investigated whether these signaling pathways are altered between MCF7 and MCF10A cells and respond to toxic polyamine supplementation. At a basal level, phosphorylated JNK and ERK1/2 were hardly detectable in MCF10A cells compared to MCF7 cells, while phosphorylated AKT levels were much higher in MCF10A cells (Figure S4). The polyamines spermidine and spermine did not cause significant changes in the phosphorylation of JNK, ERK or AKT over time (Figure S4A–H), although modest effects on JNK and AKT phosphorylation were observed (Figure S4B,D,F,H). However, MCF10A cells overexpressing ATP13A4 WT (but not D486N) and treated with spermidine (Figure 5A,B) or spermine (Figure 5C,D) presented fast and robust upregulation of JNK phosphorylation, which is reminiscent of the basal JNK phosphorylation phenotype of MCF7 cells.

Together, our findings suggest that the ATP13A4-mediated polyamine response is able to modulate the JNK signaling pathway in a time-dependent manner.

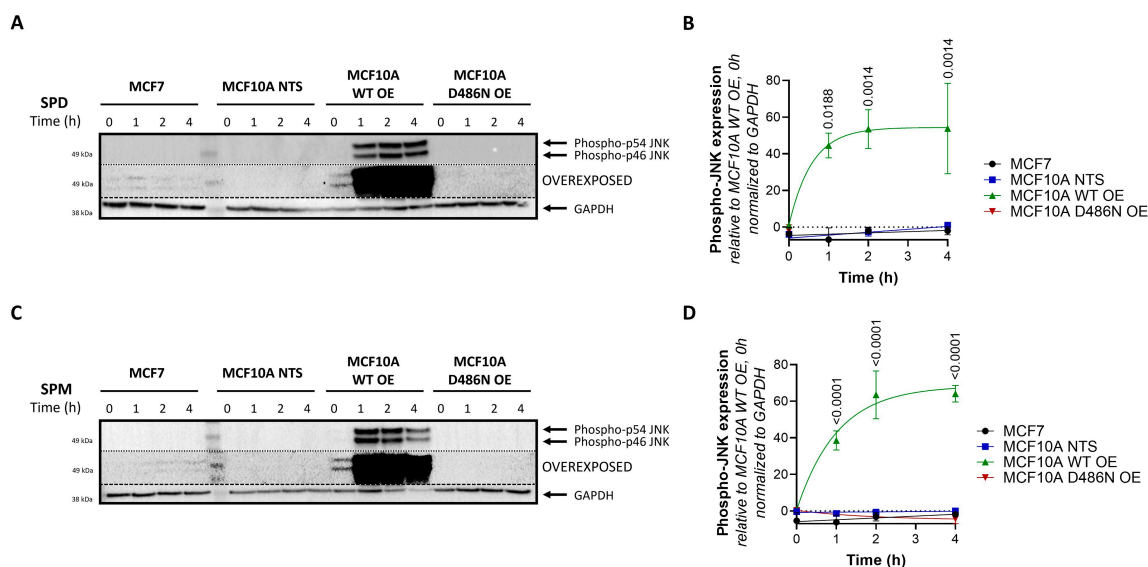


Figure 5. Overexpression of ATP13A4 WT induces JNK phosphorylation in MCF10A cells. MCF7, non-transduced (NTS) MCF10A cells and MCF10A cells overexpressing ATP13A4 WT (WT OE) or a catalytically dead mutant (D486N OE) were treated for indicated times with 100 μ M spermidine (A,B) or 100 μ M spermine (C,D). Expression levels of phospho-JNK were determined by Western blot analysis. (A,C) depict representative blots of at least three independent experiments. Of note, the blots are overexposed to show the presence of phospho-JNK bands in MCF7 cells. (B,D) show the bar graphs of the quantification of phospho-JNK levels. Data were normalized to MCF10A WT OE, an untreated control, and are presented as the mean \pm s.e.m. Statistical significance was determined by two-way ANOVA with Dunnett's multiple comparisons test, comparing the different time points to untreated controls for each cell line. *p* values are depicted in the graphs; non-significant values are not indicated.

4. Discussion

In this study, we present evidence that the elevated PTS in the commonly studied breast cancer cell line MCF7 may depend on the increased expression of ATP13A4, which we here establish as a novel polyamine transporter in the PTS that drives polyamine-dependent phenotypes in MCF7 breast cancer cells.

4.1. ATP13A4 Emerges as a Novel Polyamine Transporter in the Mammalian PTS

MCF7 cells display upregulated polyamine transport activity in comparison to MCF10A cells, which most likely is attributed to the more than 10-fold higher expression levels of ATP13A4, a previously unexplored member of the P5B-ATPases. Furthermore, we found that the overexpression of catalytically active ATP13A4 results in increased cellular polyamine uptake in MCF10A cells. These data provide the first evidence that ATP13A4 functions as a polyamine transporter in the mammalian PTS, similar to ATP13A2 and ATP13A3. The overlap in polyamine transport function among P5B-ATPases fits well with their close evolutionary relationship, the conserved biochemical behavior of spontaneous autophosphorylation, their overlapping endo-/lysosomal localization, their peculiar *N*-terminal topology and the predicted three-dimensional structures (AlphaFold) [1,31]. In addition, all P5B-ATPases present a highly conserved substrate binding site that has been resolved in human ATP13A2 [32–35] and yeast Ypk9p [36] cryo-EM structures as a polyamine binding pocket.

Fluorescently labeled polyamines are genuine substrates of P5B-ATPases stimulating their ATPase activity [19]. They behave remarkably similarly as radiolabeled polyamines for ATP13A2- or ATP13A3-dependent uptake in cells, although subtle differences have also been observed [19]. This suggests that the relative uptake capacity towards BODIPY-labeled polyamine analogs is informative but not conclusive in deducing the substrate

specificity of ATP13A4. Our data on the MCF7 and MCF10A cell models with ATP13A4 expression suggest that ATP13A4 presents broad polyamine specificity, similar to what has been described for ATP13A3 [3,19]. Indeed, we observed ATP13A4 transport-dependent BODIPY-putrescine, -spermidine and -spermine uptake that was competitive with MGBG uptake, a toxic polyamine analog. The close similarity of ATP13A4 and ATP13A3 is in line with their evolutionary relationship. ATP13A4 emerged in higher vertebrates following ATP13A3 gene duplication in the evolution of lobe-finned fish [31]. However, to unequivocally establish the polyamine specificity of ATP13A4, in-depth biochemical characterization using purified enzyme should be carried out. Whereas our results suggest that BV inhibits the PTS activity in MCF7 cells, BV did not abolish polyamine uptake in MCF10A cells overexpressing WT ATP13A4. This points to ATP13A4-independent effects of BV that may be cell-type-specific, possibly involving upstream BV-sensitive components within the endocytic pathway.

In contrast to the ubiquitously expressed ATP13A2-3 isoforms, ATP13A4 expression is tissue-specific and found mainly in epithelial glandular tissue such as the mammary glands [31], which fits well with a putative role in breast cancer. ATP13A4 has been described in early, recycling and late endosomes, overlapping to some extent with ATP13A2 and ATP13A3 localization [31]. Polyamines are first endocytosed via heparan sulphate proteoglycans [22] and are subsequently transported via various endosomal P5B ATPase isoforms towards the cytosol. Our results indicate that ATP13A4 may be (partially) redundant in function to ATP13A2 and ATP13A3, but may play a specific role in glandular cells such as the mammary glands to further boost PTS activity.

4.2. Is ATP13A4 Implicated in the Upregulated PTS of Other Cancer Types?

Besides a postulated physiological function in glandular tissue, ATP13A4 emerges as a polyamine transporter that is upregulated in MCF7 breast cancer cells, where it contributes to increased PTS activity. Follow-up studies are required to investigate whether increased ATP13A4 expression is a general hallmark of breast cancer, or whether other polyamine transporters such as ATP13A2 and ATP13A3 may also be implicated.

Many cancer types rely on an increased PTS, but it is unlikely that ATP13A4 is the only P5B-ATPase that is implicated in cancer. Indeed, ATP13A2 has been implicated in several human cancers, including melanoma [37], colon cancer [38], hepatocellular carcinoma [39], acute myeloid leukemia [40] and non-small-cell lung cancer [41], while ATP13A3 has been linked to pancreatic cancer and colorectal cancer [42–44]. Interestingly, high expression of ATP13A3 was found in metastatic pancreatic cancer cells with high polyamine uptake compared to slowly proliferating cells with low import activity [44]. Therefore, dependent on the cancer type, one or more P5B-type ATPase isoforms may be upregulated to elevate the PTS in cancerous cells.

Thus far, two other studies have highlighted a role for ATP13A4 in human cancer. The first study found an association of ATP13A4 with high-grade serous ovarian carcinoma [45], while the second study linked ATP13A4 to lung adenocarcinoma through anaplastic lymphoma kinase (ALK) rearrangements [46]. To further explore the putative role of ATP13A4 in other cancer types, we investigated the prevalence of ATP13A4 genetic alterations across various human cancers using the online database cBioPortal [47] in a pan-cancer dataset [48]. Patients with non-small-cell lung cancer showed the highest frequency of ATP13A4 alteration (>60%), with amplification as the primary genetic alteration type (Figure 6A). Of note, ATP13A4 underwent amplification in over 10% of patients with ovarian cancer, cervical cancer, head and neck cancer, endometrial cancer, uterine endometrioid carcinoma, bladder cancer, melanoma, lung cancer and breast cancer. In addition, a potential correlation between ATP13A4 genetic alterations and the clinical survival prognosis of patients was detected. Across cancers, the median overall survival time was significantly shorter for patients with ATP13A4 alterations (Figure 6B, 29.1 months versus 57.9 months for reference group). Altogether, these findings confirm that ATP13A4 alterations may be involved in cancer. To firmly establish the role of ATP13A4 in breast

cancer and other cancer types, further studies in other cancer cell models will be required to examine not only the mRNA but also the protein expression and subcellular localization of ATP13A4 and the related isoforms, ATP13A2 and ATP13A3. In addition, future knockout experiments will be essential to further corroborate the contributing roles of ATP13A4 in the upregulation of the PTS in cancer cells. This is required to validate ATP13A4 as a candidate therapeutic target for the blocking of the PTS in specific cancer types.

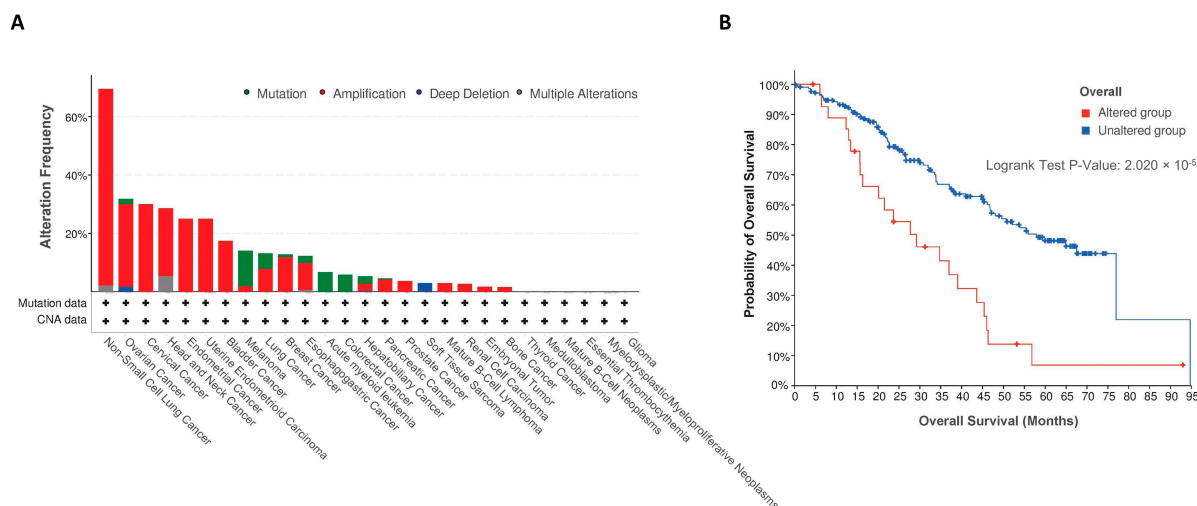


Figure 6. ATP13A4 expression in cancer. (A). Alteration frequency of ATP13A4 across different cancers from a pan-cancer dataset [48] in cBioPortal [47]. CNA, copy number alteration. (B). Overall survival analysis in cases with or without ATP13A4 alterations from the same pan-cancer dataset. Survival analysis significance was based on the log-rank test.

4.3. Interplay of ATP13A4, Polyamine Toxicity and JNK Signaling

The ATP13A4-mediated upregulation of the PTS sensitizes cells to polyamine cytotoxicity, which is a surprising finding, since cancer cell proliferation relies on elevated polyamine levels. However, our results are in line with a previous study that reported spermidine-induced apoptosis in cervical cancer [49]. We hypothesize that at high exogenous polyamine concentrations, the overactive PTS may lead to harmful intracellular polyamine accumulation that disrupts signaling, polyamine homeostasis and/or transcription and translation [50,51].

Polyamine accumulation may lead to excessive polyamine degradation with the formation of harmful reactive aldehydes and H_2O_2 [52]. However, the inhibition of the main degradative enzyme SAT1 with berenil had no differential impact on MCF7 versus MCF10A cells, indicating that the polyamine toxicity may occur independently of SAT1. Instead, the observed polyamine cytotoxicity via ATP13A4 may be mediated by the activation of the JNK pathway. We found that spermidine and spermine triggered the rapid upregulation of JNK phosphorylation in MCF10A cells that overexpressed catalytically active ATP13A4, whereas MCF7 cells exhibited high basal levels of JNK phosphorylation that responded to a lesser extent to polyamine supplementation. This difference in magnitude may be explained by the high overexpression of ATP13A4 following the lentiviral transduction of the MCF10A cells compared to the endogenous ATP13A4 levels in the MCF7 cells. Of interest, the JNK pathway has been implicated in various cancers and demonstrated to have both pro-tumorigenic and tumor-suppressive roles in breast cancer [53]. On the one hand, JNK signaling prevents tumor initiation and development in breast cancer [54,55], whereas, on the other hand, JNK activity promotes breast cancer metastasis [56,57] and contributes to tumor aggressiveness via forming an immunosuppressive tumor microenvironment [58]. ATP13A4-mediated polyamine transport may lead to sustained JNK activation with downstream apoptotic consequences.

Our observations suggest that the supplementation of polyamines to specifically induce cytotoxicity in cancer cells may be considered as a therapeutic approach, but this may not be without risk. Spermine/spermidine supplementation via drinking water appears beneficial for the longevity of model organisms without inducing cancer, but whether sufficiently high polyamine levels can be reached to induce toxicity in cells with an elevated PTS remains questionable. Furthermore, the direct injection of polyamines in rodents is lethal [59], indicating that boosting plasma polyamine levels to target cancer cells may cause adverse effects. A possibly safer alternative may be the use of toxic polyamine conjugates that preferentially enter cancer cells due to their upregulated PTS, which may be effective in inducing cell death at low concentrations [8].

In conclusion, our findings shed light on ATP13A4 as a novel member of the enigmatic PTS that is implicated in the upregulated PTS in MCF7 breast cancer cells. Future in-depth characterization of both the cytosolic and organellar impacts of ATP13A4's transport function will be instrumental in further understanding its role in (breast) cancer and may validate ATP13A4 as a candidate therapeutic target for anticancer drugs that block the PTS.

Supplementary Materials: The following supporting information can be downloaded at: <https://www.mdpi.com/article/10.3390/biom13060918/s1>, Figure S1: Benzyl viologen reduces polyamine uptake activity in MCF7 cells. The impact of benzyl viologen (BV) on cellular uptake of BODIPY-labeled putrescine (BODIPY-PUT) (A), spermidine (BODIPY-SPD) (B) and spermine (BODIPY-SPM) (C) (1 μ M, 2 h) in MCF7 versus MCF10A cells was assessed via flow cytometry. MFI, mean fluorescence intensity. (D) MCF7 and MCF10A cells were treated for 48 h with indicated concentrations of BV. Cell viability was assessed via MUH assay and data were normalized to untreated control for each cell line. Data are presented as the mean of a minimum of three independent experiments, with individual data points shown (A–C) or \pm s.e.m. (D). Statistical significance was determined by one-way ANOVA with Šídák's multiple comparisons test (A–C) or by two-way ANOVA with Šídák's multiple comparisons test (D). *p* values are depicted in the graphs. Non-significant values are not indicated in D; Figure S2: Cytotoxicity of polyamine metabolism inhibitors in MCF7 and MCF10A cells. (A) Overview of polyamine metabolism with pharmacological inhibitors indicated in red. MCF7 and MCF10A cells were treated for 1 week with indicated concentrations of DFMO (B), 4MCHA (C), APCHA (D), MGBG (E) and berenil (F). Cell viability was assessed via MUH assay. Data were normalized to untreated control for each cell line and are presented as the mean \pm s.e.m. of a minimum of three independent experiments. Statistical significance was determined by two-way ANOVA with Šídák's multiple comparisons test. *p* values are depicted in the graphs, non-significant values are not indicated. ORN: ornithine; PUT: putrescine; SPD: spermidine; SPM: spermine; ODC: ornithine decarboxylase; SRM: SPD synthase; SMS: SPM synthase; AdoMetDC: S-adenosyl-L-methionine-decarboxylase; SAT1: SPD/SPM-N(1)-acetyltransferase; DFMO: D,L-alpha-difluoromethylornithine; 4MCHA: trans-4-methylcyclohexylamine; APCHA: N-(3-aminopropyl)cyclohexylamine; MGBG: methylglyoxal bis-(guanylhydrazone); Figure S3: Benzyl viologen does not impact MCF10A cells with ATP13A4 overexpression. The impact of benzyl viologen (BV) on cellular uptake of BODIPY-labeled putrescine (BODIPY-PUT) (A), spermidine (BODIPY-SPD) (B) and spermine (BODIPY-SPM) (C) (1 μ M, 2h) in MCF10A cells (non-transduced, NTS; ATP13A4 WT overexpression, WT OE; ATP13A4 D486N mutant overexpression, D486N OE) was assessed via flow cytometry. MFI, mean fluorescence intensity. (D) MCF7 and MCF10A cells were treated for 48 h with indicated concentrations of BV. Cell viability was assessed via MUH assay and data were normalized to untreated control for each cell line. Data are presented as the mean of a minimum of three independent experiments, with individual data points shown (A–C) or \pm s.e.m. (D). Statistical significance was determined by one-way ANOVA with Šídák's multiple comparisons test (A–C) or by two-way ANOVA with Šídák's multiple comparisons test (D). *p* values are depicted in the graphs. Non-significant values are not indicated in D; Figure S4: Effects of polyamines on phosphorylation of ERK1/2, JNK and AKT in MCF7 vs. MCF10A cells. MCF7 and MCF10A cells were treated for indicated times with 100 μ M spermidine (A–D) or 100 μ M spermine (E–H). Expression levels of phospho-JNK, phospho-ERK1/2 and phospho-AKT were determined by Western blot analysis. A and E depict representative blots of at least two independent experiments, (B–D) and (F–H) show the bar graphs with the quantification. Data were normalized to MCF7, untreated control and are presented as the mean \pm s.e.m.. Statistical significance was determined by two-way ANOVA with

Dunnett's multiple comparisons test, comparing the different time points to untreated control for each cell line. Non-significant values are not indicated.

Author Contributions: Conceptualization, S.v.V. and P.V.; methodology, S.v.V., J.V.A. and C.V.d.H.; formal analysis, S.v.V.; resources, C.V.d.H.; investigation, S.v.V., A.K., E.A., J.V.A. and C.V.d.H.; writing—original draft preparation, S.v.V.; writing—review and editing, S.v.V., A.K., E.A., J.V.A., C.V.d.H., V.B., J.E. and P.V.; visualization, S.v.V.; supervision, S.v.V. and P.V.; funding acquisition, V.B. and P.V. All authors have read and agreed to the published version of the manuscript.

Funding: This research was carried out with the financial support of the Fonds voor Wetenschappelijk Onderzoek (FWO), Flanders (post-doctoral fellowship 1253721N to S.v.V. and project G094219N to P.V.), and of the KU Leuven (project C3/20/035 to P.V. and project C3/20/046 to V.B.).

Institutional Review Board Statement: Not applicable.

Informed Consent Statement: Not applicable.

Data Availability Statement: The data presented in the current study are available from the corresponding authors on reasonable request.

Acknowledgments: We would like to thank Marina Crabbe and Nathalie Jacobs for the technical support; S. Verhelst (KU Leuven) for the production of the fluorescent BODIPY polyamines; and P. Van Veldhoven (KU Leuven) for the kind gift of MGBG. We also acknowledge our frequent use of the facilities and equipment of the Cell and Tissue Imaging Cluster (P. Vanden Berghe, KU Leuven), and the FACS Core (S. Schlenner, KU Leuven). S.v.V. thanks S. Martin for his continuous support and insightful discussions.

Conflicts of Interest: The authors declare no conflict of interest.

References

1. Azfar, M.; van Veen, S.; Houdou, M.; Hamouda, N.N.; Eggermont, J.; Vangheluwe, P. P5B-ATPases in the mammalian polyamine transport system and their role in disease. *Biochim. Biophys. Acta Mol. Cell Res.* **2022**, *1869*, 119354. [[CrossRef](#)] [[PubMed](#)]
2. van Veen, S.; Martin, S.; Van den Haute, C.; Benoy, V.; Lyons, J.; Vanhoutte, R.; Kahler, J.P.; Decuyper, J.P.; Gelders, G.; Lambie, E.; et al. ATP13A2 deficiency disrupts lysosomal polyamine export. *Nature* **2020**, *578*, 419–424. [[CrossRef](#)]
3. Hamouda, N.N.; Van den Haute, C.; Vanhoutte, R.; Sannerud, R.; Azfar, M.; Mayer, R.; Cortés Calabuig, Á.; Swinnen, J.V.; Agostinis, P.; Baekelandt, V.; et al. ATP13A3 is a major component of the enigmatic mammalian polyamine transport system. *J. Biol. Chem.* **2021**, *296*, 100182. [[CrossRef](#)] [[PubMed](#)]
4. Li, J.; Meng, Y.; Wu, X.; Sun, Y. Polyamines and related signaling pathways in cancer. *Cancer Cell Int.* **2020**, *20*, 539. [[CrossRef](#)]
5. Leveque, J.; Foucher, F.; Bansard, J.Y.; Havouis, R.; Grall, J.Y.; Moulinoux, J.P. Polyamine profiles in tumor, normal tissue of the homologous breast, blood, and urine of breast cancer sufferers. *Breast Cancer Res. Treat.* **2000**, *60*, 99–105. [[CrossRef](#)] [[PubMed](#)]
6. Novita Sari, I.; Setiawan, T.; Seock Kim, K.; Toni Wijaya, Y.; Won Cho, K.; Young Kwon, H. Metabolism and function of polyamines in cancer progression. *Cancer Lett.* **2021**, *519*, 91–104. [[CrossRef](#)]
7. Corral, M.; Wallace, H.M. Upregulation of Polyamine Transport in Human Colorectal Cancer Cells. *Biomolecules* **2020**, *10*, 499. [[CrossRef](#)]
8. Palmer, A.J.; Wallace, H.M. The polyamine transport system as a target for anticancer drug development. *Amino Acids* **2010**, *38*, 415–422. [[CrossRef](#)] [[PubMed](#)]
9. Wada, M.; Canals, D.; Adada, M.; Coant, N.; Salama, M.F.; Helke, K.L.; Arthur, J.S.; Shroyer, K.R.; Kitatani, K.; Obeid, L.M.; et al. P38 delta MAPK promotes breast cancer progression and lung metastasis by enhancing cell proliferation and cell detachment. *Oncogene* **2017**, *36*, 6649–6657. [[CrossRef](#)]
10. Whyte, J.; Bergin, O.; Bianchi, A.; McNally, S.; Martin, F. Key signalling nodes in mammary gland development and cancer. Mitogen-activated protein kinase signalling in experimental models of breast cancer progression and in mammary gland development. *Breast Cancer Res.* **2009**, *11*, 209. [[CrossRef](#)]
11. Akinyele, O.; Wallace, H.M. Understanding the Polyamine and mTOR Pathway Interaction in Breast Cancer Cell Growth. *Med. Sci.* **2022**, *10*, 51. [[CrossRef](#)] [[PubMed](#)]
12. Thomas, T.J.; Thomas, T. Cellular and Animal Model Studies on the Growth Inhibitory Effects of Polyamine Analogues on Breast Cancer. *Med. Sci.* **2018**, *6*, 24. [[CrossRef](#)] [[PubMed](#)]
13. Fahrman, J.F.; Vykoukal, J.; Fleury, A.; Tripathi, S.; Dennison, J.B.; Murage, E.; Wang, P.; Yu, C.Y.; Capello, M.; Creighton, C.J.; et al. Association Between Plasma Diacetylspermine and Tumor Spermine Synthase With Outcome in Triple-Negative Breast Cancer. *J. Natl. Cancer Inst.* **2020**, *112*, 607–616. [[CrossRef](#)]
14. Rajeev, V.; Pearce, W.; Cascante, M.; Vanhaesebroeck, B.; Cutillas, P.R. Polyamine production is downstream and upstream of oncogenic PI3K signalling and contributes to tumour cell growth. *Biochem. J.* **2013**, *450*, 619–628. [[CrossRef](#)]

15. Khan, A.; Gamble, L.D.; Upton, D.H.; Ung, C.; Yu, D.M.T.; Ehteda, A.; Pandher, R.; Mayoh, C.; Hebert, S.; Jabado, N.; et al. Dual targeting of polyamine synthesis and uptake in diffuse intrinsic pontine gliomas. *Nat. Commun.* **2021**, *12*, 971. [[CrossRef](#)]
16. Soule, H.D.; Maloney, T.M.; Wolman, S.R.; Peterson, W.D., Jr.; Brenz, R.; McGrath, C.M.; Russo, J.; Pauley, R.J.; Jones, R.F.; Brooks, S.C. Isolation and characterization of a spontaneously immortalized human breast epithelial cell line, MCF-10. *Cancer Res.* **1990**, *50*, 6075–6086. [[PubMed](#)]
17. Soule, H.D.; Vazquez, J.; Long, A.; Albert, S.; Brennan, M. A human cell line from a pleural effusion derived from a breast carcinoma. *Natl. Cancer Inst.* **1973**, *51*, 1409–1416. [[CrossRef](#)]
18. Comsa, S.; Cimpean, A.M.; Raica, M. The Story of MCF-7 Breast Cancer Cell Line: 40 years of Experience in Research. *Anticancer Res.* **2015**, *35*, 3147–3154.
19. Houdou, M.; Jacobs, N.; Coene, J.; Azfar, M.; Vanhoutte, R.; Van den Haute, C.; Eggermont, J.; Daniels, V.; Verhelst, S.H.L.; Vangheluwe, P. Novel Green Fluorescent Polyamines to Analyze ATP13A2 and ATP13A3 Activity in the Mammalian Polyamine Transport System. *Biomolecules* **2023**, *13*, 337. [[CrossRef](#)]
20. Jianmongkol, S.; Vuletich, J.L.; Bender, A.T.; Demady, D.R.; Osawa, Y. Aminoguanidine-mediated inactivation and alteration of neuronal nitric-oxide synthase. *J. Biol. Chem.* **2000**, *275*, 13370–13376. [[CrossRef](#)]
21. Ding, K.; Sandgren, S.; Mani, K.; Belting, M.; Fransson, L.A. Modulations of glypican-1 heparan sulfate structure by inhibition of endogenous polyamine synthesis. Mapping of spermine-binding sites and heparanase, heparin lyase, and nitric oxide/nitrite cleavage sites. *J. Biol. Chem.* **2001**, *276*, 46779–46791. [[CrossRef](#)] [[PubMed](#)]
22. Belting, M.; Mani, K.; Jonsson, M.; Cheng, F.; Sandgren, S.; Jonsson, S.; Ding, K.; Delcros, J.G.; Fransson, L.A. Glypican-1 is a vehicle for polyamine uptake in mammalian cells: A pivotal role for nitrosothiol-derived nitric oxide. *J. Biol. Chem.* **2003**, *278*, 47181–47189. [[CrossRef](#)] [[PubMed](#)]
23. Xiao, Z.; Osipyany, A.; Song, S.; Chen, D.; Schut, R.A.; van Merkerk, R.; van der Wouden, P.E.; Cool, R.H.; Quax, W.J.; Melgert, B.N.; et al. Thieno[2,3-d]pyrimidine-2,4(1H,3H)-dione Derivative Inhibits d-Dopachrome Tautomerase Activity and Suppresses the Proliferation of Non-Small Cell Lung Cancer Cells. *J. Med. Chem.* **2022**, *65*, 2059–2077. [[CrossRef](#)] [[PubMed](#)]
24. Vanhoutte, R.; Kahler, J.P.; Martin, S.; van Veen, S.; Verhelst, S.H.L. Clickable Polyamine Derivatives as Chemical Probes for the Polyamine Transport System. *ChemBiochem* **2018**, *19*, 907–911. [[CrossRef](#)] [[PubMed](#)]
25. Konig, S.G.; Oz, S.; Kramer, R. A polyamine-modified near-infrared fluorescent probe for selective staining of live cancer cells. *Chem. Commun.* **2015**, *51*, 7360–7363. [[CrossRef](#)]
26. Lachmann, A.; Torre, D.; Keenan, A.B.; Jagodnik, K.M.; Lee, H.J.; Wang, L.; Silverstein, M.C.; Ma'ayan, A. Massive mining of publicly available RNA-seq data from human and mouse. *Nat. Commun.* **2018**, *9*, 1366. [[CrossRef](#)]
27. Blaschko, H.; Friedman, P.J.; Hawes, R.; Nilsson, K. The amine oxidases of mammalian plasma. *J. Physiol.* **1959**, *145*, 384–404. [[CrossRef](#)]
28. Kunimoto, S.; Nosaka, C.; Xu, C.Z.; Takeuchi, T. Serum effect on cellular uptake of spermidine, spergualin, 15-deoxyspergualin, and their metabolites by L5178Y cells. *J. Antibiot.* **1989**, *42*, 116–122. [[CrossRef](#)]
29. Li, H.; Prever, L.; Hirsch, E.; Gulluni, F. Targeting PI3K/AKT/mTOR Signaling Pathway in Breast Cancer. *Cancers* **2021**, *13*, 3517. [[CrossRef](#)]
30. Bhattacharya, S.; Ray, R.M.; Viar, M.J.; Johnson, L.R. Polyamines are required for activation of c-Jun NH₂-terminal kinase and apoptosis in response to TNF- α in IEC-6 cells. *Am. J. Physiol. Gastrointest. Liver Physiol.* **2003**, *285*, G980–G991. [[CrossRef](#)]
31. Sorensen, D.M.; Holemans, T.; van Veen, S.; Martin, S.; Arslan, T.; Haagendahl, I.W.; Holen, H.W.; Hamouda, N.N.; Eggermont, J.; Palmgren, M.; et al. Parkinson disease related ATP13A2 evolved early in animal evolution. *PLoS ONE* **2018**, *13*, e0193228. [[CrossRef](#)]
32. Chen, X.; Zhou, M.; Zhang, S.; Yin, J.; Zhang, P.; Xuan, X.; Wang, P.; Liu, Z.; Zhou, B.; Yang, M. Cryo-EM structures and transport mechanism of human P5B type ATPase ATP13A2. *Cell Discov.* **2021**, *7*, 106. [[CrossRef](#)]
33. Sim, S.I.; von Bulow, S.; Hummer, G.; Park, E. Structural basis of polyamine transport by human ATP13A2 (PARK9). *Mol. Cell* **2021**, *81*, 4635–4649.e8. [[CrossRef](#)]
34. Tillinghast, J.; Drury, S.; Bowser, D.; Benn, A.; Lee, K.P.K. Structural mechanisms for gating and ion selectivity of the human polyamine transporter ATP13A2. *Mol. Cell* **2021**, *81*, 4650–4662.e4. [[CrossRef](#)]
35. Tomita, A.; Daiho, T.; Kusakizako, T.; Yamashita, K.; Ogasawara, S.; Murata, T.; Nishizawa, T.; Nureki, O. Cryo-EM reveals mechanistic insights into lipid-facilitated polyamine export by human ATP13A2. *Mol. Cell* **2021**, *81*, 4799–4809.e5. [[CrossRef](#)]
36. Li, P.; Wang, K.; Salustros, N.; Gronberg, C.; Gourdon, P. Structure and transport mechanism of P5B-ATPases. *Nat. Commun.* **2021**, *12*, 3973. [[CrossRef](#)]
37. Zheng, K.; Li, T. Prediction of ATPase cation transporting 13A2 molecule in *Petromyzon marinus* and pan-cancer analysis into human tumors from an evolutionary perspective. *Immunogenetics* **2021**, *73*, 277–289. [[CrossRef](#)]
38. Chen, Q.; Zhong, L.; Zhou, C.; Feng, Y.; Liu, Q.X.; Zhou, D.; Lu, X.; Du, G.S.; Jian, D.; Luo, H.; et al. Knockdown of Parkinson's disease-related gene ATP13A2 reduces tumorigenesis via blocking autophagic flux in colon cancer. *Cell Biosci.* **2020**, *10*, 144. [[CrossRef](#)]
39. Huang, J.; Xu, S.; Yu, Z.; Zheng, Y.; Yang, B.; Ou, Q. ATP13A2 is a Prognostic Biomarker and Correlates with Immune Infiltrates in Hepatocellular Carcinoma. *J. Gastrointest. Surg.* **2023**, *27*, 56–66. [[CrossRef](#)]
40. Li, G.; Gao, Y.; Li, K.; Lin, A.; Jiang, Z. Genomic analysis of biomarkers related to the prognosis of acute myeloid leukemia. *Oncol. Lett.* **2020**, *20*, 1824–1834. [[CrossRef](#)]

41. Liu, Q.X.; Zheng, H.; Deng, X.F.; Zhou, D.; Dai, J.G. Status of the Parkinson's disease gene family expression in non-small-cell lung cancer. *World J. Surg. Oncol.* **2015**, *13*, 238. [[CrossRef](#)]
42. Li, S.; Xu, S.; Chen, Y.; Zhou, J.; Ben, S.; Guo, M.; Chu, H.; Gu, D.; Zhang, Z.; Wang, M. Metal Exposure Promotes Colorectal Tumorigenesis via the Aberrant N(6)-Methyladenosine Modification of ATP13A3. *Environ. Sci. Technol.* **2023**, *57*, 2864–2876. [[CrossRef](#)]
43. Madan, M.; Patel, A.; Skruber, K.; Geerts, D.; Altomare, D.A.; Iv, O.P. ATP13A3 and caveolin-1 as potential biomarkers for difluoromethylornithine-based therapies in pancreatic cancers. *Am. J. Cancer Res.* **2016**, *6*, 1231–1252.
44. Sekhar, V.; Andl, T.; Phanstiel, O.T. ATP13A3 facilitates polyamine transport in human pancreatic cancer cells. *Sci. Rep.* **2022**, *12*, 4045. [[CrossRef](#)]
45. Davis, S.J.; Sheppard, K.E.; Anglesio, M.S.; George, J.; Traficante, N.; Fereday, S.; Intermaggio, M.P.; Menon, U.; Gentry-Maharaj, A.; Lubinski, J.; et al. Enhanced GAB2 Expression Is Associated with Improved Survival in High-Grade Serous Ovarian Cancer and Sensitivity to PI3K Inhibition. *Mol. Cancer Ther.* **2015**, *14*, 1495–1503. [[CrossRef](#)] [[PubMed](#)]
46. Cai, C.; Long, Y.; Li, Y.; Huang, M. Coexisting of COX7A2L-ALK, LINC01210-ALK, ATP13A4-ALK and Acquired SLCO2A1-ALK in a Lung Adenocarcinoma with Rearrangements Loss During the Treatment of Crizotinib and Ceritinib: A Case Report. *OncoTargets Ther.* **2020**, *13*, 8313–8316. [[CrossRef](#)]
47. Cerami, E.; Gao, J.; Dogrusoz, U.; Gross, B.E.; Sumer, S.O.; Aksoy, B.A.; Jacobsen, A.; Byrne, C.J.; Heuer, M.L.; Larsson, E.; et al. The cBio cancer genomics portal: An open platform for exploring multidimensional cancer genomics data. *Cancer Discov.* **2012**, *2*, 401–404. [[CrossRef](#)]
48. The ICGC/TCGA Pan-Cancer Analysis of Whole Genomes Consortium. Pan-cancer analysis of whole genomes. *Nature* **2020**, *578*, 82–93. [[CrossRef](#)]
49. Chen, Y.; Zhuang, H.; Chen, X.; Shi, Z.; Wang, X. Spermidine-induced growth inhibition and apoptosis via autophagic activation in cervical cancer. *Oncol. Rep.* **2018**, *39*, 2845–2854. [[CrossRef](#)]
50. Poulin, R.; Pelletier, G.; Pegg, A.E. Induction of apoptosis by excessive polyamine accumulation in ornithine decarboxylase-overproducing L1210 cells. *Biochem. J.* **1995**, *311 Pt 3*, 723–727. [[CrossRef](#)]
51. Sakamoto, A.; Sahara, J.; Kawai, G.; Yamamoto, K.; Ishihama, A.; Uemura, T.; Igarashi, K.; Kashiwagi, K.; Terui, Y. Cytotoxic Mechanism of Excess Polyamines Functions through Translational Repression of Specific Proteins Encoded by Polyamine Modulon. *Int. J. Mol. Sci.* **2020**, *21*, 2406. [[CrossRef](#)]
52. Murray Stewart, T.; Dunston, T.T.; Woster, P.M.; Casero, R.A., Jr. Polyamine catabolism and oxidative damage. *J. Biol. Chem.* **2018**, *293*, 18736–18745. [[CrossRef](#)] [[PubMed](#)]
53. Wu, Q.; Wu, W.; Jacevic, V.; Franca, T.C.C.; Wang, X.; Kuca, K. Selective inhibitors for JNK signalling: A potential targeted therapy in cancer. *J. Enzyme Inhib. Med. Chem.* **2020**, *35*, 574–583. [[CrossRef](#)] [[PubMed](#)]
54. Girnius, N.; Edwards, Y.J.; Garlick, D.S.; Davis, R.J. The cJUN NH(2)-terminal kinase (JNK) signaling pathway promotes genome stability and prevents tumor initiation. *eLife* **2018**, *7*, e36389. [[CrossRef](#)]
55. Itah, Z.; Chaudhry, S.; Raju Ponny, S.; Aydemir, O.; Lee, A.; Cavanagh-Kyros, J.; Tournier, C.; Muller, W.J.; Davis, R.J. HER2-driven breast cancer suppression by the JNK signaling pathway. *Proc. Natl. Acad. Sci. USA* **2023**, *120*, e2218373120. [[CrossRef](#)]
56. Insua-Rodriguez, J.; Pein, M.; Hongu, T.; Meier, J.; Descot, A.; Lowy, C.M.; De Braekeleer, E.; Sinn, H.P.; Spaich, S.; Sutterlin, M.; et al. Stress signaling in breast cancer cells induces matrix components that promote chemoresistant metastasis. *EMBO Mol. Med.* **2018**, *10*, e9003. [[CrossRef](#)]
57. Pein, M.; Insua-Rodriguez, J.; Hongu, T.; Riedel, A.; Meier, J.; Wiedmann, L.; Decker, K.; Essers, M.A.G.; Sinn, H.P.; Spaich, S.; et al. Metastasis-initiating cells induce and exploit a fibroblast niche to fuel malignant colonization of the lungs. *Nat. Commun.* **2020**, *11*, 1494. [[CrossRef](#)]
58. Semba, T.; Wang, X.; Xie, X.; Cohen, E.N.; Reuben, J.M.; Dalby, K.N.; Long, J.P.; Phi, L.T.H.; Tripathy, D.; Ueno, N.T. Identification of the JNK-Active Triple-Negative Breast Cancer Cluster Associated With an Immunosuppressive Tumor Microenvironment. *J. Natl. Cancer Inst.* **2022**, *114*, 97–108. [[CrossRef](#)] [[PubMed](#)]
59. Tabor, C.W.; Rosenthal, S.M. Pharmacology of spermine and spermidine; some effects on animals and bacteria. *J. Pharmacol. Exp. Ther.* **1956**, *116*, 139–155. [[PubMed](#)]

Disclaimer/Publisher's Note: The statements, opinions and data contained in all publications are solely those of the individual author(s) and contributor(s) and not of MDPI and/or the editor(s). MDPI and/or the editor(s) disclaim responsibility for any injury to people or property resulting from any ideas, methods, instructions or products referred to in the content.